High-Resolution Estimation of Multidimensional Spectra from Unevenly Sampled Data

Butt, Naveed; Jakobsson, Andreas

Published in:
Digital Signal Processing (DSP), 2011 17th International Conference on

DOI:
10.1109/ICDSP.2011.6004971

2011

HIGH-RESOLUTION ESTIMATION OF MULTIDIMENSIONAL SPECTRA FROM UNEVENLY SAMPLED DATA

Naveed R. Butt and Andreas Jakobsson

Center For Mathematical Sciences, Lund University
Box 118, SE 22100, Lund, Sweden
Phone: + (46) 46 22 285 50, fax: + (46) 46 22 246 23
Email: naveed@maths.lth.se; andreas.jakobsson@matstat.lu.se

ABSTRACT

Estimation of high-resolution multidimensional spectra from unevenly sampled limited sized data sets plays an important role in a large variety of signal processing applications. In this work, we develop a high-resolution non-parametric estimator for unevenly sampled N-dimensional data based on a recently introduced iterative method, the so-called iterative adaptive approach (IAA). The proposed estimator uses the definition of the multidimensional Fourier transform to obtain a frequency domain representation of the unevenly sampled signal. Using tensor algebra, the multidimensional frequency domain representation is then recast into matrix format and used in a weighted least squares (WLS) fitting criterion to iteratively obtain estimates of the spectral amplitudes and the covariance matrix. The proposed estimator is numerically shown to provide superior performance as compared to the commonly used least squares Fourier transform (LSFT) estimator.

Index Terms— Multidimensional spectra, estimation, weighted least squares.

1. INTRODUCTION

Estimation of high-resolution multidimensional spectra plays an important role in a large variety of signal processing applications, covering fields such as geophysics, biomedicine, image processing, sonar and radar systems, nuclear resonance, telecommunications and economics (see, e.g., [1] and references therein). In many of these applications, the multidimensional signal may be unevenly sampled or may suffer from lost samples in one or more dimensions (see, e.g., [2–6]). Due to their inherent robustness to model assumptions, non-parametric estimators of multidimensional spectra are of particular importance. However, the commonly used non-parametric methods for missing data cases are generally based on the multidimensional least squares Fourier transform (LSFT) [3]. The LSFT has been shown to be a modified version of the periodogram and to have the same statistical properties as the periodogram for the evenly-sampled case [3]. Due to this, the multidimensional LSFT estimator inherits the performance limitations of the periodogram, and fails to provide high-resolution estimates for small sized data sets. On the other hand, the well known high-resolution estimators, such as Capon and APES [7], are applicable only for uniform sampling. There is, therefore, a pressing need to develop non-parametric estimators for multidimensional spectra that provide accurate estimates for unevenly sampled data. In this work, we develop a non-parametric estimator for unevenly sampled N-dimensional data based on the recently introduced iterative method, the so-called iterative adaptive approach (IAA), that has been shown to provide high-resolution estimates of the power spectrum [8] and the magnitude squared coherence (MSC) [9] for both uniformly sampled and non-uniformly sampled one-dimensional data. The proposed estimator, here termed the N-dimensional IAA (ND-IAA), uses the definition of the multidimensional Fourier transform to obtain a frequency domain representation of the unevenly sampled signal. Using tensor algebra, the multidimensional frequency domain representation is then recast into matrix format and used in a weighted least squares (WLS) fitting criterion to iteratively obtain estimates of the spectral amplitudes and the covariance matrix. The proposed estimator is numerically shown to provide superior performance as compared to the commonly used LSFT estimator.

This paper is organized as follows; in the next section, we present the generalized N-dimensional data model covering the uneven sampling case. In Section 3, we develop the proposed ND-IAA estimator. The performance of the proposed estimator is evaluated numerically in Section 4.

Notational notes: We represent scalars with small letters in light-face, e.g., x, vectors with small letters in bold-face, e.g., $\mathbf{x}$, matrices with capital letters in bold-face, e.g., $\mathbf{X}$, and tensors with capital letters in bold Euler script, e.g., $\boldsymbol{\mathcal{X}}$. The transpose and the complex conjugate transpose are represented as $(\cdot)^T$ and $(\cdot)^*$, respectively.

2. N-DIMENSIONAL DATA MODEL

A given, N-dimensional, unevenly measured, data set may be represented by an N-way tensor $\boldsymbol{\mathcal{X}} \in \mathbb{C}^{I_1 \times I_2 \times \cdots \times I_N}$, whose element $(i_1, i_2, \ldots, i_N)$ is denoted as

$$x_{t_{i_1}^{(1)}, t_{i_2}^{(2)}, \ldots, t_{i_N}^{(N)}}, \tag{1}$$

where $i_n = 1, \ldots, I_n;\ n = 1, \ldots, N$. Here, to allow for an uneven sampling along one or more dimensions, the sampling times along any of the dimensions, $\{t_{i_n}^{(n)}\}_{i_n=1}^{I_n}$, are not required to be uniformly spaced. We note that this arrangement also covers the case of uniformly sampled data, as well as if such a set include missing samples. Furthermore, selecting a $K_1 \times K_2 \times \cdots \times K_N$ frequency grid whose corresponding frequencies along any dimension, say dimension r, are given as

$$\{\omega_{k_r}^{(r)}\}_{k_r=1}^{K_r}, \quad r = 1, \ldots, N, \tag{2}$$

and using the definition of the N-dimensional Fourier transform [10], a grid-dependent frequency-domain representation of (1)

This work was supported in part by the Swedish Research Council and Carl Trygger's foundation, Sweden.

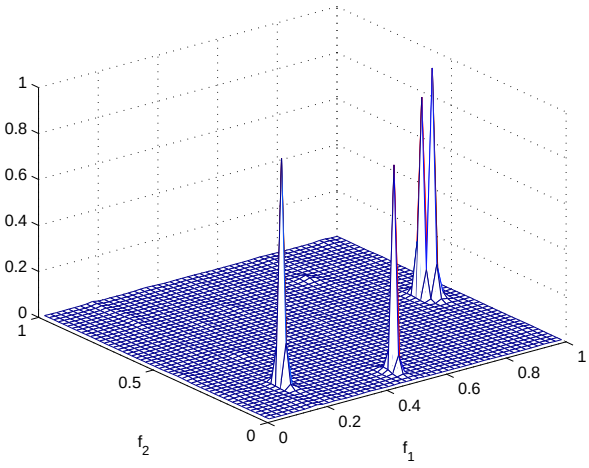

Fig. 1. Spectral estimate using ND-IAA for SNR = 4 dB, $M = 10$.

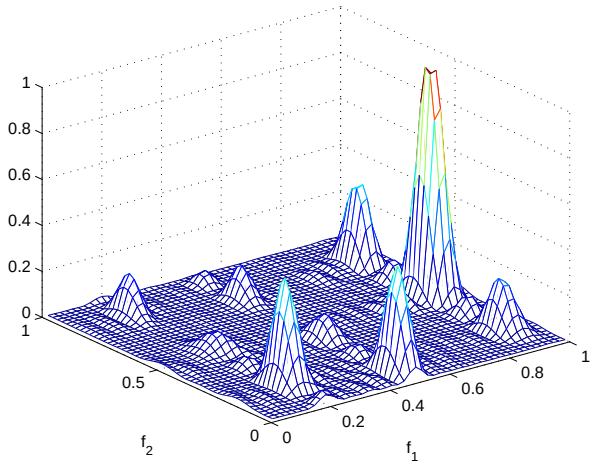

Fig. 2. Spectral estimate using LSFT for SNR = 4 dB, $M = 10$.

may be formed as (3), shown on the top of the next page, where $i_n = 1, \ldots, I_n$; $n = 1, \ldots, N$, and $\alpha(\omega_{k_1}^{(1)}, \omega_{k_2}^{(2)}, \ldots, \omega_{k_N}^{(N)})$ represents the (unknown) complex-valued spectral amplitude at the $(k_1, k_2, \ldots, k_N)$-th frequency grid point, including any corrupting noise elements. It should be stressed that no signal model has been assumed in forming the representation in (3); rather the signal is seen as the contribution corresponding to each (multidimensional) frequency grid point. There is thus no corrupting noise terms as is typical in model-based methods describing the data as a signal and a noise part. Instead the contribution of any noise component, or any other interference, is implicitly described via its contribution to $\alpha(\omega_{k_1}^{(1)}, \omega_{k_2}^{(2)}, \ldots, \omega_{k_N}^{(N)})$.

3. THE PROPOSED ND-IAA ALGORITHM

A compact representation of (3) may be obtained by defining an N-way tensor, $\mathcal{G} \in \mathbb{C}^{K_1 \times K_2 \times \cdots \times K_N}$, whose element $(k_1, k_2, \ldots, k_N)$ is the spectral amplitude $\alpha(\omega_{k_1}^{(1)}, \omega_{k_2}^{(2)}, \ldots, \omega_{k_N}^{(N)})$. Further, defining

$$\mathbf{a}^{(n)}(\omega_{k_n}^{(n)}) = \left[\begin{array}{ccc} e^{j\omega_{k_n}^{(n)} t_1^{(n)}} & \ldots & e^{j\omega_{k_n}^{(n)} t_{I_n}^{(n)}} \end{array} \right]^T \quad (4)$$

$$\mathbf{A}^{(n)} = \left[\begin{array}{ccc} \mathbf{a}^{(n)}(\omega_1^{(n)}) & \ldots & \mathbf{a}^{(n)}(\omega_{K_n}^{(n)}) \end{array} \right], \quad (5)$$

where $\mathbf{a}^{(n)}(\omega_{k_n}^{(n)})$ represents the Fourier vector corresponding to the sampling times along the n-th dimension (or parameter) at the frequency $\omega_{k_n}^{(n)}$, and $\mathbf{A}^{(n)} \in \mathbb{C}^{I_n \times K_n}$ the corresponding Fourier matrix, leads to the tensor representation of (3) being formed as (see [11] for details)

$$\mathcal{X} = \mathcal{G} \times_1 \mathbf{A}^{(1)} \times_2 \mathbf{A}^{(2)} \cdots \times_N \mathbf{A}^{(N)}, \quad (6)$$

where the operator $\times_n$ represents the n-mode product of a tensor with a matrix. The data tensor, $\mathcal{X}$, may now be matricized using the Kronecker product as (see, e.g., [11], [12]),

$$\mathbf{X}_{(1)} = \mathbf{A}^{(1)} \mathbf{G}_{(1)} \left(\mathbf{A}^{(N)} \otimes \mathbf{A}^{(N-1)} \otimes \cdots \otimes \mathbf{A}^{(2)} \right)^T, \quad (7)$$

where $\otimes$ represents the Kronecker product, and the matrix $\mathbf{X}_{(1)} \in \mathbb{C}^{I_1 \times (\prod_{n=2}^{N} I_n)}$ is obtained by horizontally stacking all the mode-1 slices of $\mathcal{X}$.[1] The matrix $\mathbf{G}_{(1)} \in \mathbb{C}^{K_1 \times (\prod_{n=2}^{N} K_n)}$ is defined similarly. Finally, using the property that for any conformable matrices $\mathbf{Z}, \mathbf{D}, \mathbf{E}, \mathbf{F}$ (see, e.g., [13]),

$$\mathbf{Z} = \mathbf{D}\mathbf{E}\mathbf{F}^T \quad \Leftrightarrow \quad \text{vec}\,(\mathbf{Z}) = (\mathbf{F} \otimes \mathbf{D})\text{vec}\,(\mathbf{E}), \quad (8)$$

where vec$(\cdot)$ represents the vectorization operator , one may express the vector form of (7)

$$\text{vec}\,\left(\mathbf{X}_{(1)}\right) = \left(\mathbf{A}^{(N)} \otimes \cdots \otimes \mathbf{A}^{(2)} \otimes \mathbf{A}^{(1)} \right) \text{vec}\,\left(\mathbf{G}_{(1)}\right). \quad (9)$$

For notational convenience, rewrite (9) as

$$\mathbf{y} = \mathbf{B}\mathbf{g}, \quad (10)$$

where

$$\mathbf{y} \triangleq \text{vec}\,\left(\mathbf{X}_{(1)}\right) \in \mathbb{C}^{\tilde{I} \times 1} \quad (11)$$

$$\mathbf{g} \triangleq \text{vec}\,\left(\mathbf{G}_{(1)}\right) \in \mathbb{C}^{\tilde{K} \times 1} \quad (12)$$

$$\mathbf{B} \triangleq \left(\mathbf{A}^{(N)} \otimes \cdots \otimes \mathbf{A}^{(2)} \otimes \mathbf{A}^{(1)} \right) \in \mathbb{C}^{\tilde{I} \times \tilde{K}}, \quad (13)$$

where $\tilde{I} = \prod_{n=1}^{N} I_n$, and $\tilde{K} = \prod_{n=1}^{N} K_n$. Using (10), one may form the covariance matrix of $\mathbf{y}$ as

$$\mathbf{R} \triangleq \sum_{\ell=1}^{\tilde{K}} |g_\ell|^2 \mathbf{b}_\ell \mathbf{b}_\ell^*, \quad (14)$$

where g_ℓ and $\mathbf{b}_\ell$ represent the ℓ-th element of $\mathbf{g}$ and the ℓ-th column of $\mathbf{B}$, respectively. Furthermore, following the weighted-least

[1] The matricization may be easiest understood with an example. Consider a tensor $\mathcal{X} \in \mathbb{R}^{3 \times 4 \times 2}$, whose mode-1 slices are

$$\mathbf{X}_1 = \left[\begin{array}{cccc} 1 & 2 & 3 & 4 \\ 5 & 6 & 7 & 8 \\ 9 & 10 & 11 & 12 \end{array} \right], \quad \mathbf{X}_2 = \left[\begin{array}{cccc} 13 & 14 & 15 & 16 \\ 17 & 18 & 19 & 20 \\ 21 & 22 & 23 & 24 \end{array} \right].$$

Then the mode-1 matricization of $\mathcal{X}$ is

$$\mathbf{X}_{(1)} = \left[\begin{array}{cccccccc} 1 & 2 & 3 & 4 & 13 & 14 & 15 & 16 \\ 5 & 6 & 7 & 8 & 17 & 18 & 19 & 20 \\ 9 & 10 & 11 & 12 & 21 & 22 & 23 & 24 \end{array} \right].$$

$$x_{t_{i_1}^{(1)},t_{i_2}^{(2)},\ldots,t_{i_N}^{(N)}} = \sum_{k_1=1}^{K_1}\sum_{k_2=1}^{K_2}\cdots\sum_{k_N=1}^{K_N}\alpha(\omega_{k_1}^{(1)},\omega_{k_2}^{(2)},\ldots,\omega_{k_N}^{(N)})\, e^{j\omega_{k_1}^{(1)}t_{i_1}^{(1)}}\cdots e^{j\omega_{k_N}^{(N)}t_{i_N}^{(N)}}, \tag{3}$$

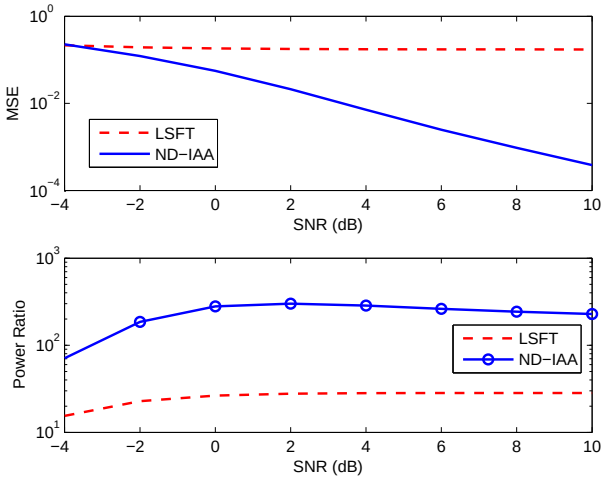

Fig. 3. Top: MSE of the peak at (0.2,0.2) as a function of the SNR, for $M = 8$. Bottom: Power ratio as a function of the SNR, for $M = 8$.

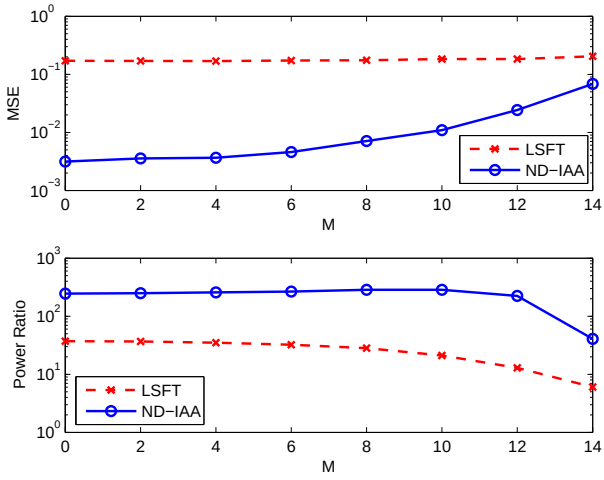

Fig. 4. Top: MSE of the peak at (0.2,0.2) as a function of M, for SNR = 4. Bottom: Power ratio as a function of M, for SNR = 4 dB.

squares approach of [8], one may then form the estimates of g_ℓ and $\mathbf{R}$ iteratively, as

$$\hat{g}_\ell = \frac{\mathbf{b}_\ell^*\hat{\mathbf{R}}^{-1}\mathbf{y}}{\mathbf{b}_\ell^*\hat{\mathbf{R}}^{-1}\mathbf{b}_\ell} \tag{15}$$

$$\hat{\mathbf{R}} = \sum_{\ell=1}^{\bar{K}}|\hat{g}_\ell|^2\mathbf{b}_\ell\mathbf{b}_\ell^*, \tag{16}$$

with $\hat{\mathbf{R}}$ being initialized to the identity matrix. The converged estimates of the spectral amplitudes in (15) may be used to form the estimate $\hat{\mathbf{g}}$, which upon reshuffling, leads to the estimate of the spectral amplitude tensor $\hat{\mathcal{G}}$. Finally, using $\hat{\mathcal{G}}$, the N-dimensional power spectrum of $\mathcal{X}$ is estimated as

$$\hat{\mathcal{P}} = \text{conj}\left(\hat{\mathcal{G}}\right)\odot\hat{\mathcal{G}}, \tag{17}$$

where conj$(\cdot)$ represents complex conjugation, and $\odot$ the Hadamard element-wise product.

4. NUMERICAL EXAMPLES

In this section, we examine the performance of the proposed ND-IAA estimator using simulated 2-D and 3-D data. For the first set of simulations, we generate 2-D complex data representing four sinusoids in noise

$$x_{t_{i_1}^{(1)},t_{i_2}^{(2)}} = \sum_{l=1}^{4}\alpha_l e^{2\pi j\nu_l}e^{2\pi j(f_l^{(1)}t_1^{(1)}+f_l^{(2)}t_2^{(2)})} + w_{t_{i_1}^{(1)},t_{i_2}^{(2)}},$$

where $f_l^{(1)}$ and $f_l^{(2)}$ denote the two frequencies of the lth 2-D sinusoid, while α_l represents its complex amplitude; ν_l is a uniformly distributed random variable between 0 and 2π, representing the phase; and the noise term,$w_{t_{i_1}^{(1)},t_{i_2}^{(2)}}$ is a zero-mean circularly symmetric Gaussian random process. In the simulations, we set $\alpha_l = 1, \forall l$, and the true peaks at $(0.2, 0.2), (0.5, 0.1), (0.9, 0.5)$ and $(0.92, 0.48)$. To simulate a scenario of uniform sampling along $t^{(1)}$ and uneven sampling along $t^{(2)}$, we set $\{t_1^{(1)}, t_2^{(1)}, \ldots, t_{I_1}^{(1)}\} = \{1, 2, \ldots, I_1\}$, while $\{t_1^{(2)}, t_2^{(2)}, \ldots, t_{I_2-M}^{(2)}\}$ are picked randomly for each simulation from $\{1, 2, \ldots, I_2\}$, where $M < I_2$. The total number of available samples is, therefore, $I_1 \times (I_2 - M)$. For this study, we set $I_1 = I_2 = 16$, while M is increased from 0 to 14 in steps of 2. A frequency grid of 50×50 points is used. It is worth stressing that as the examined approaches are non-parametric, no assumptions of model order or noise color or distribution are needed. The results of the numerical study are shown in Figures 1-4. Figures 1 and 2 show typical 3-D plots of the spectral estimate using the proposed ND-IAA method and the commonly used least squares Fourier transform (LSFT) method, respectively, for $M = 6$ and a signal-to-noise ratio (SNR) of 4 dB. As is clear from the figures, the ND-IAA estimator substantially outperforms the LSFT estimator which fails to resolve the closely-spaced peaks at (0.9,0.5) and (0.92,0.48). The LSFT estimator is also seen to suffer from several spurious peaks. For further analysis, we compare two performance measures for the estimators, namely, the mean squared error (MSE) of the first peak, and the power ratio of the estimated spectra. Here, we define the power ratio as the ratio of the power of the four peaks to the power of the off-peak spectrum. Thus, the power ratio provides a good measure for the amount of spurious peaks or off-peak noise that is known to appear in LSFT estimators. Both the MSE and the power ratio are estimated from 300 independent Monte Carlo

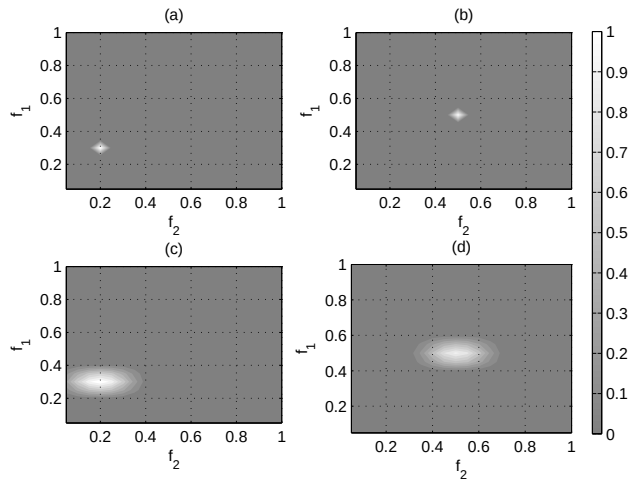

Fig. 5. Power spectrum estimates for 3-D data at SNR = 6 dB. (a) ND-IAA, $f_3 = 0.1$, (b) ND-IAA, $f_3 = 0.5$, (c) LSFT, $f_3 = 0.1$, (d) LSFT, $f_3 = 0.5$. True peaks at (0.3,0.2,0.1) and (0.5,0.5,0.5).

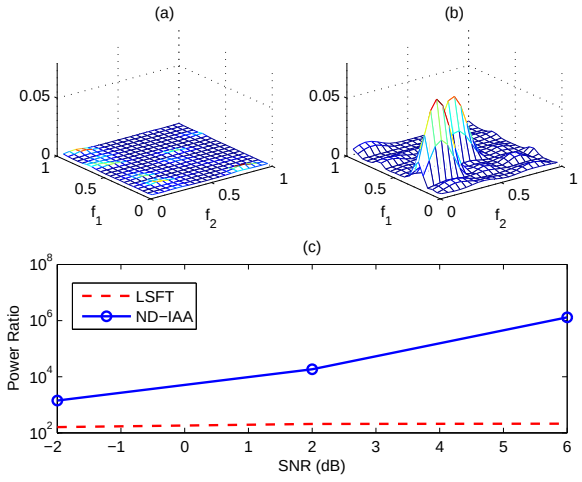

Fig. 6. Power spectrum estimates for 3-D data at SNR = 6 dB, showing typical off-peak planes and the overall power ratio. (a) ND-IAA, $f_3 = 0.7$, (b) LSFT, $f_3 = 0.7$. (c) Power ratio as a function of SNR.

simulations for different selections of SNR and M. In each run, the noise and the pattern of uneven sampling along $t^{(2)}$ vary independently. Figure 3 shows the MSE and the power ratio as a function of SNR for $M = 6$. As is clear from the two plots in Figure 3, the proposed estimator gives quite a high gain in the power ratio for all SNR levels, while its MSE performance improves with increasing SNR. Finally, Figure 4 shows the MSE and the power ratio as a function of M for SNR = 4 dB. Recall that the number of available samples is $16 \times (16 - M)$, which decreases significantly as M increases from 0 to 14. As before, the ND-IAA estimator outperforms the LSFT estimator, making it highly suitable for high-resolution estimation of multidimensional spectra from possibly unevenly sampled data.

The proposed algorithm was also tested on 3-D data, similar to the 2-D data, having two complex sinusoids in white Gaussian noise. The true peaks were set at $(0.3, 0.2, 0.1)$ and $(0.5, 0.5, 0.5)$. Figure 5 shows typical power spectrum estimates obtained through ND-IAA (subplots (a),(b)) and LSFT (subplots (c),(d)) algorithms for the two planes containing the true peaks (a 'plane' here represents a 2-D slice of the three dimensional frequency axis taken along the frequency in the third dimension, e.g., Figure 5(a) shows the frequency plane $(f_1, f_2, 0.1)$). The results show clearly that the ND-IAA estimates provide much sharper peaks as compared to LSFT, at the expected locations. Since LSFT is known to suffer from spurious peaks, we also studied the power distribution in the off-peak planes. Plots (a) and (b) in Figure 6 show the spectral estimates in a typical off-peak plane (i.e., a plane at frequency f_3 not containing any spectral peak) for ND-IAA and LSFT algorithms, respectively. It is evident from the plots that ND-IAA algorithm allows very little off-peak power as compared to LSFT. Finally, Figure 6 (c) shows that the low off-peak noise allowed by ND-IAA results in a significant gain in the power ratio as compared to LSFT.

5. REFERENCES

[1] J. H. McClellan, "Multidimensional Spectral Estimation," *Proc. IEEE*, vol. 70, pp. 1029–1037, September 1982.

[2] A. Afifi and R. Elashoff, "Missing observations in multivariate statistics I: Review of the literature," *J. Amer. Statist. Assoc.*, pp. 595–604, 1966.

[3] J. D. Scargle, "Studies in astronomical time series analysis. ii. statistical aspects of spectral analysis of unevenly spaced data," *The Astrophysical Journal*, vol. 263, pp. 835–853, 1982.

[4] Thomas P. Bronez, "Spectral estimation of irregularly sampled mutildimensional processes by generalized prolate spheroidal sequences," *IEEE Transactions on Acoustics, Speech and Signal Processing*, vol. 36, no. 12, pp. 1862–1873, December 1988.

[5] M. Schulz and K. Stattegger, "Spectrum: Spectral analysis of unevenly spaced paleoclimatic time series," *Computers and Geosciences*, vol. 23, no. 9, pp. 929–945, 1997.

[6] Y. Wang, J. Li, and P. Stoica, *Spectral Analysis of Signals, The Missing Data Case*, USA: Morgan & Claypool Publishers, 2005.

[7] P. Stoica and R. Moses, *Spectral Analysis of Signals*, Pearson Prentice Hall, Upper Saddle River, NJ, 2005.

[8] T. Yardibi, J. Li, P. Stoica, M. Xue, and A. B. Baggeroer, "Source localization and sensing: A nonparametric iterative adaptive approach based on weighted least squares," *IEEE Transactions on Aerospace and Electronic Systems. In Press.*, 2009.

[9] Naveed R. Butt and Andreas Jakobsson, "Coherence spectrum estimation from non-uniformly sampled sequences," *IEEE Signal Processing Letters*, vol. 17, no. 4, pp. 339–342, April 2010.

[10] Ian Naismith Sneddon, *Fourier Transforms*, Dover Publications, Inc. N.Y., 1995.

[11] Tamara G. Kolda and Brett W. Bader, "Tensor decomposition and applications," *SIAM Review*, vol. 51, no. 3, pp. 455–500, 2009.

[12] R. L. Bishop and S. I. Goldberg, *Tensor Analysis on Manifolds*, Dover Publications, Inc., New York, 1968.

[13] R. A. Horn and C. A. Johnson, *Topics in Matrix Analysis*, Cambridge University Press, Cambridge, England, 1991.